2024 10th IEEE RAS/EMBS International Conference for
Biomedical Robotics and Biomechatronics (BioRob)
1-4 September 2024. Heidelberg, Germany

2024 10th IEEE RAS/EMBS International Conference for Biomedical Robotics and Biomechatronics (BioRob) | 979-8-3503-8652-3/24/$31.00 ©2024 IEEE | DOI: 10.1109/BIOROB60516.2024.10719820

Task-Dependent Sonomyographic Features Extracted from Task-Independent Factorization are Sensitive to Ambulation Scenario

Juliana R. Iverson, *Member, IEEE,* Kaitlin G. Rabe, *Member, IEEE,* and Nicholas P. Fey, *Member, IEEE*

***Abstract*—Leg prostheses exist that can recreate complex functional movements. However, these devices often lack intuitive methods for control and evaluation for specific users. Sonomyography is the dynamic ultrasound imaging of skeletal muscle and a user-specific signal able to image surface and deep tissue. Various forms of decomposition have been applied to muscle-based sensing to understand the underlying motor control of individuals during motion (e.g., non-negative matrix factorization (NNMF) on electromyography). The purpose of this study was to apply NNMF to sonomyography from differing ambulation modes. We hypothesized that pooled (i.e., task-independent) output of NNMF can be used to extract task-dependent (i.e., ambulation-dependent) features. Nine individuals completed overground ambulation trials over level ground, as well as ramp (10°) and stair (35°) ascent/descent. Sonomyography was collected from the quadriceps and hamstrings. NNMF (with 4 control signals) was applied to these data, after it was parsed for all strides and averaged across ambulation modes, resulting in matrices of spatial weights and temporal control signals for each participant. The inverse of the weighting matrix was next multiplied by sonomyographic data from each ambulation mode, to produce "recovered" control signals. Correlations were computed between these signals across modes to test our hypothesis, which we accepted. Across modes, each respective control signal appeared to be unique with respect to each other. We conclude that NNMF of sonomyography is a useful method to reduce its dimensionality and recover signal features for sensing user intent of lower-extremity wearable devices (e.g., leg prostheses) or to assess the motor control strategy used by individuals.**

I. Introduction

People affected by lower limb loss wish to be able to ambulate without added cognitive load on all types of terrains and surfaces [1]. Currently-available passive prostheses can aid quality of life for lower-limb amputees. However, these devices typically do not return full mobility and can also lead to orthopedic and/or cognitive issues such as osteoarthritis in the sound limb of users [2]. Active (i.e., robotic) leg prostheses have been developed and tested, often with the intention of improving mobility, decreasing energetic demand and reducing asymmetric joint loading [3]. Lower-limb prosthetic research has delivered active, and in some instances passive, prostheses able to replicate natural lower limb motion. If controlled by a microprocessor, these devices as well as upper-limb devices often lack intuitive methods of control [4,5]. Synchronizing the neuromotor control strategy of the user to the control system of the prosthesis has been a goal, which is typically enabled through a myoelectric control system. These systems usually predict user intention (or intended motion) by interpreting surface electromyography (EMG). Conventional methods for recording EMG can be limited by low signal to noise ratio, crosstalk between neighboring muscles, sensitivity to socket conditions and little ability to record signals beyond superficial musculature [5-8]. In terms of previous work, among veterans with amputations, myoelectric upper-extremity prostheses have not led to an increase in functionality or satisfaction and were the most rejected type of active prosthesis with the chief reason being "too much fuss" [9,10], which highlights that there is an essential balance between complexity of the devices (and its controller) and the utility of the device as perceived by specific patients. For both upper- and lower-extremity prostheses, there is a need to continue to develop robust and accurate methods for sensing user intent, especially when motor tasks are complex, such as using a prosthesis to ambulate during different scenarios.

Sonomyography is the dynamic ultrasound imaging of skeletal muscle. The grayscale intensity, or the echogenicity, with values ranging from 0 to 255, for standard sonomyography images is related to the acoustic impedance of tissues and provides information about the composition of superficial and deep muscles and surrounding tissues [11,12]. Previous upper- and lower-limb research has shown that muscle cross sectional area, tissue stiffness, muscle contractions and muscle fatigue can be recovered from transverse and longitudinal B-mode or 3D sonomyography data [13-17]. Previous work has also shown that sonomyography performs just as well as and, in some instances, better than EMG for lower-limb movement classification and continuous joint kinematic prediction [14-17]. These predictions have been provided by a number of different features extracted from sonomyography as well as associate classifier and algorithm architectures such as Bayesian, parametric and neural networks, to name a few. For example, these approaches when applied to sonomyography, produce temporal and spatial features through methods such as an averaged vector set of time-intensity features over the whole image [14], linear curve fitting on a sparse set of scan lines from individual ultrasound

*Research was supported by NSF grant #2054343.

J. R. Iverson is with the Walker Department of Mechanical Engineering at The University of Texas at Austin, Austin, TX 78712 USA (e-mail: jiverson@utexas.edu).

K. G. Rabe is with the Department of Biomedical Engineering at the University of Texas at Austin, TX 78712 USA (e-mail: kaitlin.rabe@utexas.edu).

N. P. Fey is with the Walker Department of Mechanical Engineering at The University of Texas at Austin, Austin, TX 78712 USA (e-mail: nfey@utexas.edu).

images [15], principal component analysis [16,17], aggregate image differences across motion [18], as well as aponeurosis and fascicle tracking [19].

Non-negative matrix factorization (NNMF) is a mathematical technique that transforms one matrix of data into two matrices: a weighting matrix and a matrix of time- or phase-varying control signals, with the number of control signals being chosen as an optimization parameter *a priori*. For example, NNMF has been applied to EMG in order to reveal reduced sets of muscle synergies that "work together" to explain or create complex motion [20-22]. NNMF has also been successfully implemented with EMG to create reduced dimensional data for robust motion prediction [23,24]. The purpose of this study was to apply NNMF to sonomyographic data of differing ambulation modes. We hypothesized that pooled (i.e., task-independent) output of NNMF decomposition can be used to extract task-dependent features that significantly differ based on ambulation mode. This strategy could be useful to guide personalizable control systems of wearable assistive devices, as well as to understand how the motor control strategy of an individual is affected by specific ambulation modes (i.e., the user environment) or a given design/control property of a device.

II. Methods

A. Data Collection

Nine able-bodied subjects performed two sets of five ambulation tasks for one-minute. Subjects performed self-selected speed level walking as well as 10° incline and decline walking on a force instrumented treadmill (Bertec, Columbus, OH, USA). Subjects also performed stair ascent and descent on an ambulation circuit with a 35° grade 4-stair staircase. A custom 3D printed ultrasound probe holder was used to center the transducer flush across the belly of the rectus femoris (anterior) in a transverse orientation for one trial, and then the biceps femoris longhead (posterior) for the next trial on the left leg of each subject. The depth of the image was set to provide a full view of the tissue from the surface of the limb to the femur. In the anterior condition, these images recorded data from the vastus lateralis, vastus intermedius and rectus femoris. In the posterior condition, these images recorded data from the biceps femoris longhead, biceps femoris shorthead and the semitendinosus. Sonomyography data were collected with a 128-element linear array transducer with a center frequency of 7.5 MHz at varying scan depths based on the anatomy of the subject ranging from 50–70mm. Whole-body kinematics were recorded using VICON 3D (Vicon, Oxford, UK) motion capture with reflective markers. Heel strike and toe off events were labeled in Visual3D (C-Motion Inc, Boyds, MD, USA) software. All data was synchronized and further processed using custom MATLAB (Mathworks, Natick, MA, USA) code. Posterior data for 2 subjects was insufficient for analyses due to sensor lift off. Therefore, the analysis of the anterior data included all 9 subjects and the analysis for the posterior data included 7 subjects.

B. Sonomyography Analysis

The ultrasound images were analyzed using a pipeline from the raw sonomyography data to its filtering and pooling across ambulation modes, as well as the application of NNMF (Fig 1). Each sonomyography frame was first processed with a 3mm x 3mm averaging filter applied to the whole image. A 1D array was created from the average blocks ordering the rows of blocks from the top of the image down. Toe off events were used to create individual gait cycles from frames of ultrasound data. As shown in Fig. 1, each stride was represented as a matrix [B x F] where F is the number of frames in one stride and B is the number of averaged blocks in a frame for that subject's scan depth. Each subjects' strides were then interpolated across the stride and each interpolation was then averaged to create a new matrix [B x t] that represented the average stride of each subject for each ultrasound view for each of the five ambulation modes. The stride matrices created from each ambulation mode were combined and averaged together, or pooled, within each ultrasound view and for each subject.

An unsupervised NNMF routine was applied to these task-independent pooled strides. Using the nnmf function in

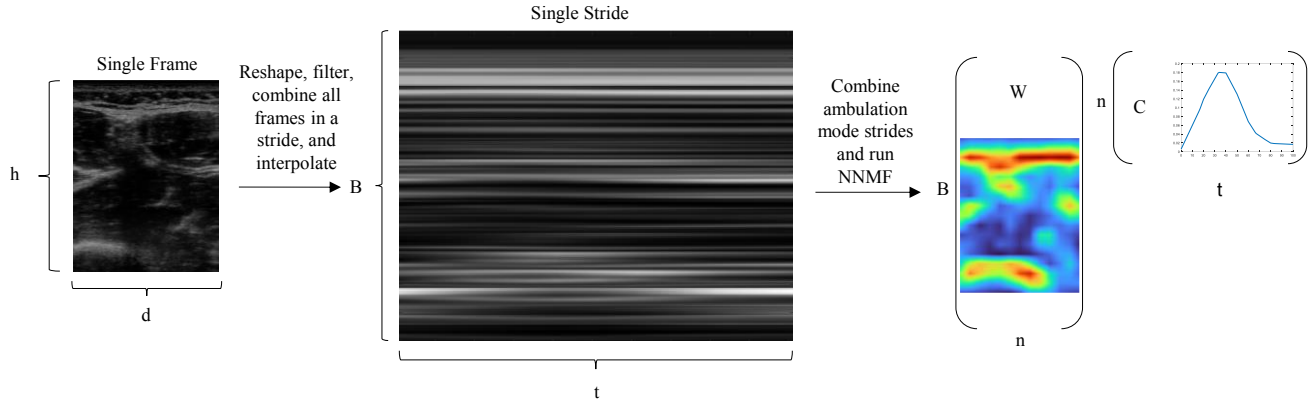

Figure 1. A 3mm x 3mm averaging filter was applied to each ultrasound image, creating a number of average blocks, B, that represent each frame. Each filtered ultrasound frame was then processed to create a 1D array from the 2D image. Frames in one stride were combined together as columns then interpolated to the highest number of frames captured in a stride across all trials. Average strides were created for each ambulation mode, which were then averaged together to create one overall average stride. NNMF was then applied to this average stride to create a spatial weighting matrix (W) of size B x n and a temporal control signal matrix (C) of size n x t.

MATLAB, the pooled strides were decomposed into 4 temporal control signal arrays and 4 spatial weightings arrays. Residuals were calculated after the NNMF decomposition. The number of control signals was based on the uni- and bi-articular nature of imaged muscles, as well as the influence of active and passive force generation of these muscle tissues. The mode-independent weighting arrays along with task-dependent average stride ultrasounds were

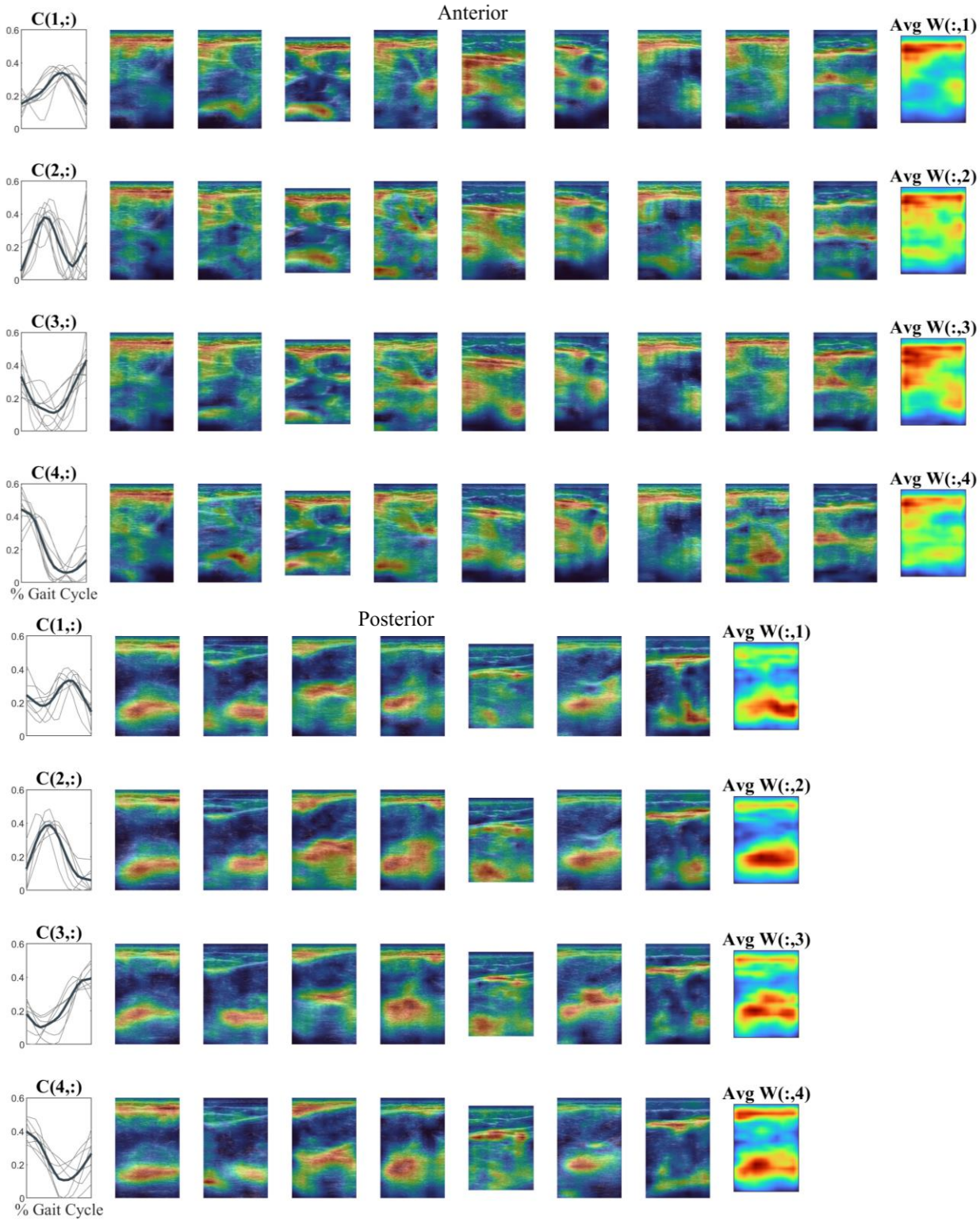

Figure 2. The NNMF decomposition of the pooled task-independent sonomyography data reveals spatial weightings (W's) and temporal control signals (C's). The bold line in the control signal graphs is the average among subjects and the thin lines are the actual subject control signal values. The heat maps are the columns of the weighting array reorganized to the correct 2D dimensions and overlaid on a subject's ultrasound image and are normalized to the highest weighting value for each individual array. The average heat map is to show trends in spatial weightings but is not used in further analysis.

used to recover ambulation mode specific control signals. A pseudoinverse of the pooled weighting array was created with the pinv function in MATLAB. This pseudoinverse was then multiplied by the ambulation mode specific stride to recover ambulation mode specific control signals for each subject for each ultrasound view. In order to show the differences between the ambulation modes in the resulting recovered control signals, Pearson correlation coefficients were computed for each ultrasound view. Each set of control signals were compared to the like control signals for each ultrasound view as a method for assessing signal similarity.

III. Results

The NNMF decomposition well represented the data of the pooled stride for each ultrasound view for each subject. The average residual for the anterior view was 0.0015 with a standard deviation of 0.0004 and the average residual for the posterior view was 0.0013 with a standard deviation of 0.0003 as well. The heat maps were created for visualization (Fig. 2) and generally, these elements of the weight matrix corresponded well with the changes in echogenicity of the original images. The spatial weightings significantly differ between the anterior and posterior muscle results. The pooled control signals appear similar, yet distinct for the anterior and posterior muscle analyses. The recovered control signals (Fig. 3) also appear similar between the anterior and posterior views. The highest correlations (Table I) were most often between walking signals and incline and decline signals, and lowest between walking and stairs. Both incline and decline walking signals show greater agreement with level-ground walking signals than with each other. Stair ascent and descent showed the least agreement with the other ambulation modes across control signals. No correlation coefficients across all control signals across ambulation modes averaged above 0.800.

IV. Discussion

The purpose of this study was to apply NNMF to sonomyographic data of differing ambulation modes. We hypothesized that pooled (i.e., task-independent) output of NNMF decomposition can be used to extract task-dependent features that significantly differ based on ambulation mode. We accept this hypothesis using the results in Table I that show the different correlation coefficients between the recovered signals across different ambulation modes.

A. Non-Negative Matrix Factorization

By visually inspecting the control signals, the anterior and

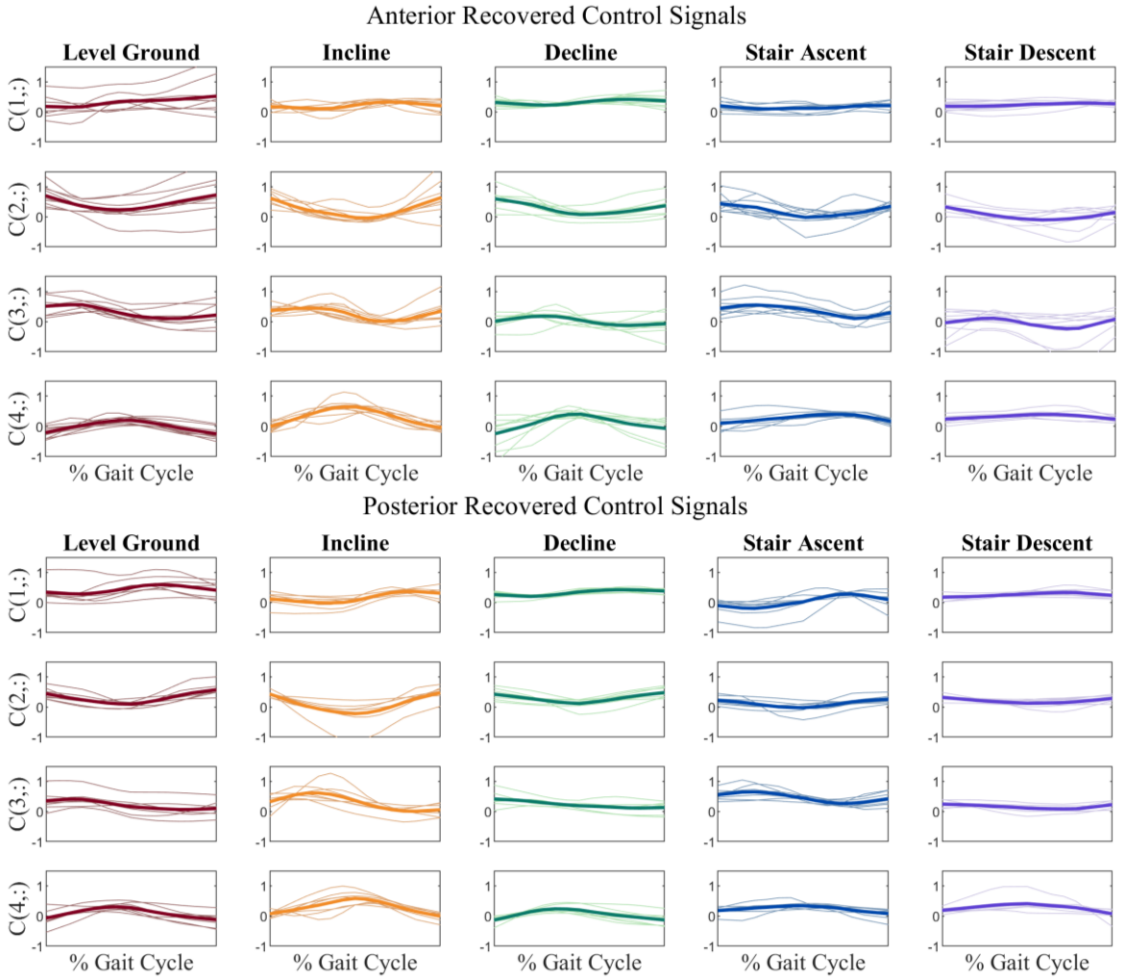

Figure 3. The recovered ambulation mode specific control signals are grouped vertically by ambulation mode and horizontally by similar control signals. The bold line is the group average and the thin lines represent subject specific recovered control signals.

TABLE I.

Anterior Recovered Control Signal Average Correlation Coefficients

	Walking *C(1,:)*	Incline *C(1,:)*	Decline *C(1,:)*	Stair Ascent *C(1,:)*	Stair Descent *C(1,:)*
Walking *C(1,:)*	1.000	0.605 (0.432)	0.341 (0.468)	0.207 (0.820)	0.147 (0.670)
Incline *C(1,:)*	0.605 (0.432)	1.000	0.309 (0.666)	0.217 (0.729)	-0.040 (0.753)
Decline *C(1,:)*	0.341 (0.468)	0.309 (0.666)	1.000	0.433 (0.446)	0.149 (0.706)
Stair Ascent *C(1,:)*	0.207 (0.820)	0.217 (0.729)	0.433 (0.446)	1.000	0.012 (0.598)
Stair Descent *C(1,:)*	0.147 (0.670)	-0.040 (0.753)	0.149 (0.706)	0.012 (0.598)	1.000

	Walking *C(2,:)*	Incline *C(2,:)*	Decline *C(2,:)*	Stair Ascent *C(2,:)*	Stair Descent *C(2,:)*
Walking *C(2,:)*	1.000	0.776 (0.191)	0.455 (0.558)	0.490 (0.423)	0.242 (0.467)
Incline *C(2,:)*	0.776 (0.191)	1.000	0.635 (0.278)	0.591 (0.274)	0.560 (0.454)
Decline *C(2,:)*	0.455 (0.558)	0.635 (0.278)	1.000	0.573 (0.400)	0.684 (0.390)
Stair Ascent *C(2,:)*	0.490 (0.423)	0.591 (0.274)	0.573 (0.400)	1.000	0.441 (0.478)
Stair Descent *C(2,:)*	0.242 (0.467)	0.560 (0.454)	0.684 (0.390)	0.441 (0.478)	1.000

	Walking *C(3,:)*	Incline *C(3,:)*	Decline *C(3,:)*	Stair Ascent *C(3,:)*	Stair Descent *C(3,:)*
Walking *C(3,:)*	1.000	0.761 (0.337)	0.362 (0.701)	0.591 (0.474)	0.605 (0.269)
Incline *C(3,:)*	0.761 (0.337)	1.000	0.350 (0.727)	0.452 (0.412)	0.625 (0.305)
Decline *C(3,:)*	0.362 (0.701)	0.350 (0.727)	1.000	0.406 (0.521)	0.466 (0.442)
Stair Ascent *C(3,:)*	0.591 (0.474)	0.452 (0.412)	0.406 (0.521)	1.000	0.339 (0.518)
Stair Descent *C(3,:)*	0.605 (0.269)	0.625 (0.305)	0.466 (0.442)	0.339 (0.518)	1.000

	Walking *C(4,:)*	Incline *C(4,:)*	Decline *C(4,:)*	Stair Ascent *C(4,:)*	Stair Descent *C(4,:)*
Walking *C(4,:)*	1.000	0.792 (0.357)	0.842 (0.119)	0.454 (0.301)	0.669 (0.292)
Incline *C(4,:)*	0.792 (0.357)	1.000	0.719 (0.307)	0.439 (0.406)	0.524 (0.514)
Decline *C(4,:)*	0.842 (0.119)	0.719 (0.307)	1.000	0.405 (0.343)	0.617 (0.362)
Stair Ascent *C(4,:)*	0.454 (0.301)	0.439 (0.406)	0.405 (0.343)	1.000	0.525 (0.442)
Stair Descent *C(4,:)*	0.669 (0.292)	0.524 (0.514)	0.617 (0.362)	0.525 (0.442)	1.000

Posterior Recovered Control Signal Average Correlation Coefficients

	Walking *C(1,:)*	Incline *C(1,:)*	Decline *C(1,:)*	Stair Ascent *C(1,:)*	Stair Descent *C(1,:)*
Walking *C(1,:)*	1.000	0.496 (0.606)	0.541 (0.519)	0.711 (0.369)	0.754 (0.219)
Incline *C(1,:)*	0.496 (0.606)	1.000	0.641 (0.271)	0.761 (0.164)	0.283 (0.651)
Decline *C(1,:)*	0.541 (0.519)	0.641 (0.271)	1.000	0.811 (0.153)	0.415 (0.567)
Stair Ascent *C(1,:)*	0.711 (0.369)	0.761 (0.164)	0.811 (0.153)	1.000	0.494 (0.584)
Stair Descent *C(1,:)*	0.754 (0.219)	0.283 (0.651)	0.415 (0.567)	0.494 (0.584)	1.000

	Walking *C(2,:)*	Incline *C(2,:)*	Decline *C(2,:)*	Stair Ascent *C(2,:)*	Stair Descent *C(2,:)*
Walking *C(2,:)*	1.000	0.830 (0.202)	0.813 (0.375)	0.646 (0.173)	0.596 (0.281)
Incline *C(2,:)*	0.830 (0.202)	1.000	0.901 (0.076)	0.815 (0.078)	0.688 (0.205)
Decline *C(2,:)*	0.813 (0.375)	0.901 (0.076)	1.000	0.748 (0.168)	0.457 (0.169)
Stair Ascent *C(2,:)*	0.646 (0.173)	0.815 (0.078)	0.748 (0.168)	1.000	0.679 (0334)
Stair Descent *C(2,:)*	0.596 (0.281)	0.688 (0.205)	0.457 (0.169)	0.679 (0334)	1.000

	Walking *C(3,:)*	Incline *C(3,:)*	Decline *C(3,:)*	Stair Ascent *C(3,:)*	Stair Descent *C(3,:)*
Walking *C(3,:)*	1.000	0.778 (0.368)	0.671 (0.442)	0.486 (0.618)	0.461 (0.480)
Incline *C(3,:)*	0.778 (0.368)	1.000	0.485 (0.708)	0.686 (0.272)	0.537 (0.314)
Decline *C(3,:)*	0.671 (0.442)	0.485 (0.708)	1.000	0.536 (0.370)	0.253 (0.437)
Stair Ascent *C(3,:)*	0.486 (0.618)	0.686 (0.272)	0.536 (0.370)	1.000	0.434 (0.416)
Stair Descent *C(3,:)*	0.461 (0.480)	0.537 (0.314)	0.253 (0.437)	0.434 (0.416)	1.000

	Walking *C(4,:)*	Incline *C(4,:)*	Decline *C(4,:)*	Stair Ascent *C(4,:)*	Stair Descent *C(4,:)*
Walking *C(4,:)*	1.000	0.696 (0.292)	0.840 (0.263)	0.627 (0.280)	0.705 (0.283)
Incline *C(4,:)*	0.696 (0.292)	1.000	0.653 (0.405)	0.630 (0.347)	0.662 (0.263)
Decline *C(4,:)*	0.840 (0.263)	0.653 (0.405)	1.000	0.576 (0.399)	0.785 (0.143)
Stair Ascent *C(4,:)*	0.627 (0.280)	0.630 (0.347)	0.576 (0.399)	1.000	0.474 (0.483)
Stair Descent *C(4,:)*	0.705 (0.283)	0.662 (0.263)	0.785 (0.143)	0.474 (0.483)	1.000

a. The results of averaging the correlation coefficients of each subject's recovered Cs with the other respective ambulation mode recovered Cs. The standard deviations for the correlation coefficient averages are reported in the parentheses. These correlation coefficients support our hypothesis that the recovered control signals are sensitive to ambulation mode.

posterior views are distinct yet similar. Thus, while the two views show different musculature cross sections, similar characteristics of the motion appears to be provided by both views. This makes sense considering the quadriceps and hamstrings both contain biarticular and uniarticular muscle tissue that can alter their tension through active (i.e., modulated neural drive) or passive mechanisms. We also noticed there is a similarity between the shape of the pooled control signals and known biomechanical measures such as hip and knee angles and moments that have been previously reported [e.g., 25]. The heat maps show agreement with anatomical landmarks in the subject specific ultrasound frames. The echogenicity of an ultrasound is directly related to the physical properties of the underlying tissues therefore we believe the decomposed pooled weights are also related to mechanisms of force generation (either actively or passively) within the tissue, but are relatively invariant within a stride and across modes of ambulation. Thus, we conclude that this unsupervised mathematical decomposition technique, when applied to sonomyography, produces user-specific and anatomically-relevant spatial and phase-varying features of ambulation.

B. Recovered Ambulation Mode Specific Control Signals

The recovered control signals appear quite similar, but the results in Table I show that they are indeed distinct from one another. The results are consistent with our hypothesis that we could use NNMF with task-independent and task-dependent sonomyography to recover ambulation mode specific control signals. There is evidence that features from sonomyography data allow for proportional control of upper limb robotic prostheses [26,27]. The similar appearance of the recovered control signals, yet different correlation coefficients support the idea that sonomyography data has the ability to be used for proportional control of intended lower-limb motion. The incline and decline walking control signals show better agreement with level ground walking signals than the stair ascent and descent for both anterior and posterior views, supporting the idea that the signals contain information about the motion that is mode specific. It also makes sense when considering the relatively shallow grade of the ramps (10°) versus the stair (35°) conditions and/or the range of motion of the hip and knee to achieve ambulation on these terrains [e.g., 28]

C. Future Work and Applications

Extracting features from sonomyography to improve user intent prediction accuracy is a growing area of research. Much of this research focuses solely on the upper limb [6,8]. The work presented here is the first time NNMF has been used to reduce dimensionality of lower-limb transverse sonomyography and extract ambulation-specific features. The NNMF decomposition creates two distinct sets of output: the pooled control signals and the pooled weightings. Future work could analyze the sonomyography control signals for correlations with joint kinematics and how the signals are related to the intended limb movement. Future work could also analyze the relationship between the weighting matrix and underlying anatomy. Limitations of this work include a discrete set of ambulation types, and relatively modest number of subjects per ultrasound view. Future work could be done using NNMF on sonomyography from various placements and orientations along the lower limb during more widely-varying scenarios. This study was also performed on able bodied individuals. Sonomyography data from patients [e.g., 29] is also an important area of

future work.

V. Conclusion

The work presented here shows that a data rich 2D sonomyography signal can be well represented temporally and spatially as a select number of control signals and weightings using NNMF. This decomposition contains user-specific anatomical information in the form of a weighting matrix that can then be used with user-specific and task-dependent sonomyography data to recover control signals that are sensitive to ambulation mode. These control signals are temporal features extracted from sonomyography data that could be of use for lower-limb user intent prediction, or a targeted characterization of specific motor control responses used by individuals.

References

[1] S. Manz et al., "A review of user needs to drive the development of lower limb prostheses," Journal of NeuroEngineering and Rehabilitation, vol. 19, no. 1, p. 119, Nov. 2022, doi: 10.1186/s12984-022-01097-1.

[2] R. Gailey, K. Allen, J. Castles, J. Kucharik, and M. Roeder, "Review of secondary physical conditions associated with lower-limb amputation and long-term prosthesis use," *J Rehabil Res Dev*, vol. 45, no. 1, pp. 15–29, 2008.

[3] S. Farrokhi, B. Mazzone, A. Yoder, K. Grant, and M. Wyatt, "A Narrative Review of the Prevalence and Risk Factors Associated With Development of Knee Osteoarthritis After Traumatic Unilateral Lower Limb Amputation," *Military Medicine*, vol. 181, 2016.

[4] E. J. Wolf *et al.*, "Advanced technologies for intuitive control and sensation of prosthetics," *Biomed Eng Lett*, vol. 10, no. 1, pp. 119–128, Aug. 2019.

[5] D. Farina *et al.*, "The extraction of neural information from the surface EMG for the control of upper-limb prostheses: emerging avenues and challenges," *IEEE Trans Neural Syst Rehabil Eng*, vol. 22, no. 4, pp. 797–809, Jul. 2014.

[6] M. Windrich, M. Grimmer, O. Christ, S. Rinderknecht, and P. Beckerle, "Active lower limb prosthetics: a systematic review of design issues and solutions," *Biomed Eng Online*, vol. 15, 2016.

[7] A. Cimolato, J. J. M. Driessen, L. S. Mattos, E. De Momi, M. Laffranchi, and L. De Michieli, "EMG-driven control in lower limb prostheses: a topic-based systematic review," *Journal of NeuroEng and Rehabil*, vol. 19, 2022.

[8] A. Fleming, N. Stafford, S. Huang, X. Hu, D. P. Ferris, and H. (Helen) Huang, "Myoelectric control of robotic lower limb prostheses: a review of electromyography interfaces, control paradigms, challenges and future directions," *J. Neural Eng.*, vol. 18, 2021

[9] G. M. Berke et al., "Comparison of satisfaction with current prosthetic care in veterans and servicemembers from Vietnam and OIF/OEF conflicts with major traumatic limb loss," *JRRD*, vol. 47, 2010.

[10] R. Gailey et al., "Unilateral lower-limb loss: Prosthetic device use and functional outcomes in servicemembers from Vietnam war and OIF/OEF conflicts," *JRRD*, vol. 47, 2010.

[11] K. M. Meiburger, U. R. Acharya, and F. Molinari, "Automated localization and segmentation techniques for B-mode ultrasound images: A review," *Computers in Biology and Medicine*, vol. 92, pp. 210–235, Jan. 2018.

[12] F. Sarto, J. Spörri, D. P. Fitze, J. I. Quinlan, M. V. Narici, and M. V. Franchi, "Implementing Ultrasound Imaging for the Assessment of Muscle and Tendon Properties in Elite Sports: Practical Aspects, Methodological Considerations and Future Directions," *Sports Med*, vol. 51, no. 6, pp. 1151–1170, Jun. 2021.

[13] M. Salvi, C. Caresio, K. M. Meiburger, B. De Santi, F. Molinari, and M. A. Minetto, "Transverse Muscle Ultrasound Analysis (TRAMA): Robust and Accurate Segmentation of Muscle Cross-Sectional Area," *Ultrasound in Medicine & Biology*, vol. 45, no. 3, pp. 672–683, Mar. 2019.

[14] K. G. Rabe, M. H. Jahanandish, J. R. Boehm, A. Majewicz Fey, K. Hoyt, and N. P. Fey, "Ultrasound Sensing Can Improve Continuous Classification of Discrete Ambulation Modes Compared to Surface Electromyography," *IEEE Transactions on Biomedical Engineering*, vol. 68, no. 4, pp. 1379–1388, Apr. 2021.

[15] Y. Huang, X. Yang, Y. Li, D. Zhou, K. He, and H. Liu, "Ultrasound-Based Sensing Models for Finger Motion Classification," *IEEE Journal of Biomedical and Health Informatics*, vol. 22, no. 5, pp. 1395–1405, Sep. 2018.

[16] S. Engdahl *et al.*, "Classification Performance and Feature Space Characteristics in Individuals With Upper Limb Loss Using Sonomyography," *IEEE J Transl Eng Health Med*, vol. 10, p. 2100311, 2022.

[17] S. Engdahl, A. Dhawan, G. Lévay, A. Bashatah, R. Kaliki, and S. Sikdar, "Motion prediction using electromyography and sonomyography for an individual with transhumeral limb loss." medRxiv, Dec. 26, 2020.

[18] N. Akhlaghi *et al.*, "Real-Time Classification of Hand Motions Using Ultrasound Imaging of Forearm Muscles," *IEEE Trans Biomed Eng*, vol. 63, no. 8, pp. 1687–1698, Aug. 2016, doi: 10.1109/TBME.2015.2498124.

[19] M. H. Jahanandish, N. P. Fey, and K. Hoyt, "Lower-Limb Motion Estimation Using Ultrasound Imaging: A Framework For Assistive Device Control," *IEEE J Biomed Health Inform*, vol. 23, no. 6, pp. 2505–2514, Nov. 2019, doi: 10.1109/JBHI.2019.2891997.

[20] D. J. Clark, L. H. Ting, F. E. Zajac, R. R. Neptune, and S. A. Kautz, "Merging of Healthy Motor Modules Predicts Reduced Locomotor Performance and Muscle Coordination Complexity Post-Stroke," *Journal of Neurophysiology*, vol. 103, no. 2, pp. 844–857.

[21] L. H. Ting and J. M. Macpherson, "A limited set of muscle synergies for force control during a postural task," *J Neurophysiol*, vol. 93, no. 1, pp. 609–613, Jan. 2005.

[22] R. L. Routson, S. A. Kautz, and R. R. Neptune, "Modular organization across changing task demands in healthy and poststroke gait," *Physiol Rep*, vol. 2, no. 6, p. e12055, Jun. 2014.

[23] H. Dimitrov, A. M. J. Bull, and D. Farina, "Real-Time Interface Algorithm for Ankle Kinematics and Stiffness From Electromyographic Signals," *IEEE Transactions on Neural Systems and Rehabilitation Engineering*, vol. 28, no. 6, pp. 1416–1427, Jun. 2020.

[24] N. Jiang, K. B. Englehart, and P. A. Parker, "Extracting Simultaneous and Proportional Neural Control Information for Multiple-DOF Prostheses From the Surface Electromyographic Signal," *IEEE Transactions on Biomedical Engineering*, vol. 56, no. 4, pp. 1070–1080, Apr. 2009.

[25] R. Riener, M. Rabuffetti, and C. Frigo, "Stair ascent and descent at different inclinations," Gait & Posture, vol. 15, no. 1, pp. 32–44, Feb. 2002.

[26] S. Patwardhan, J. Schofield, W. M. Joiner, and S. Sikdar, "Sonomyography shows feasibility as a tool to quantify joint movement at the muscle level," *IEEE Int Conf Rehabil Robot*, vol. 2022, pp. 1–5, Jul. 2022.

[27] S. Sikdar *et al.*, "Novel Method for Predicting Dexterous Individual Finger Movements by Imaging Muscle Activity Using a Wearable Ultrasonic System," *IEEE Trans Neural Syst Rehabil Eng*, vol. 22, no. 1, pp. 69–76, Jan. 2014.

[28] R. M. Neuman and N. P. Fey, "There are unique kinematics during locomotor transitions between level ground and stair ambulation that persist with increasing stair grade," Sci Rep, vol. 13, no. 1, p. 8576, May 2023.

[29] J. Mendez, R. Murray, L. Gabert, N. P. Fey, H. Liu, and T. Lenzi, "Continuous A-Mode Ultrasound-Based Prediction of Transfemoral Amputee Prosthesis Kinematics Across Different Ambulation Tasks," IEEE Trans Biomed Eng, vol. 71, no. 1, pp. 56–67, Jan. 2024.